Precision measurements of a simple chaotic circuit

Ken Kiers[a] and Dory Schmidt[b]
Department of Physics, Taylor University, Upland, Indiana 46989

J. C. Sprott[c]
Department of Physics, University of Wisconsin, Madison, Wisconsin 53706

(Received 10 June 2003; accepted 27 August 2003)

We describe a simple nonlinear electrical circuit that can be used to study chaotic phenomena. The circuit employs simple electronic elements such as diodes, resistors, and operational amplifiers, and is easy to construct. A novel feature of the circuit is its use of an almost ideal nonlinear element, which is straightforward to model theoretically and leads to excellent agreement between experiment and theory. For example, comparisons of bifurcation points and power spectra give agreement to within 1%. The circuit yields a broad range of behavior and is well suited for qualitative demonstrations and as a serious research tool.
[DOI: 10.1119/1.1621031]

I. INTRODUCTION

The study of nonlinear systems and chaos provides a fascinating gateway into the world of research for students. With the growing use of nonlinear analysis techniques in many areas of science, it also is becoming increasingly important to provide undergraduate students with a good introduction to nonlinear systems. Undergraduate chaos experiments that are available commercially tend either to be relatively expensive or to be somewhat qualitative in nature. Many articles have been published over the past 15 years regarding chaotic behavior in systems ranging from a bouncing ball to various electronic circuits.[1–8] In many of these articles the authors have made clever use of low cost or readily available equipment to illustrate well-known aspects and analytical techniques associated with chaos, such as bifurcation diagrams, periodic and chaotic attractors, return maps and Poincaré sections.

Nonlinear electronic circuits provide an excellent tool for the study of chaotic behavior. Some of these circuits treat time as a discrete variable, employing sample-and-hold subcircuits and analog multipliers to model iterated maps such as the logistic map.[1] Continuous-time flows are somewhat easier to model electronically. One of the best-known chaotic circuits of this latter type is Chua's circuit.[9–11] The original version of this circuit contains an inductor (making it difficult to model and to scale to different frequencies), but inductorless versions of Chua's circuit have also been described.[12–14] Recent work has highlighted several new chaotic circuits that are very simple to construct and analyze.[15,16] These circuits correspond to simple third-order differential equations, are easy to scale to different frequencies, and contain only simple electronic elements such as diodes, operational amplifiers (op amps), and resistors. Furthermore, with slight modifications, they hold the potential for very precise comparisons between theory and experiment.[17] The differential equations corresponding to these circuits are among the simplest third-order differential equations that lead to chaotic behavior.[18–22] As noted in Refs. 16 and 17, several of these circuits may be grouped together and regarded as an analog computer for the precise experimental study of chaotic phenomena. Some possible uses of these circuits involve studies of synchronization[23] and secure communication.[24] Furthermore, several such circuits could in principle be linked together to investigate higher-dimensional chaos.

One class of simple circuits that leads to chaotic behavior is described by the following third-order differential equation,[17]

$$\dddot{x} = -A\ddot{x} - \dot{x} + D(x) - \alpha, \tag{1}$$

where x represents the voltage at a particular node in the corresponding circuit. In Eq. (1) A and α are constants, the dots denote derivatives with respect to a dimensionless time, and $D(x)$ is a nonlinear function that characterizes the nonlinearity in the circuit.

In this paper we describe an investigation of a new circuit belonging to the class of circuits described by Eq. (1). The nonlinearity in the circuit models a function proportional to $\min(x,0)$. The circuit is similar to the one described in Ref. 15, but uses a more precise implementation of the nonlinearity.[25] The increase in precision allows for a detailed comparison between theory and experiment. Such comparisons yield agreement to within 1% for quantities such as bifurcation points. The data taken from the circuit also can be used in a variety of ways to illustrate many aspects of chaotic and periodic behavior.

The paper is structured as follows. In Sec. II we describe the circuit and provide several technical details. Section III contains the experimental results and compares these to theoretical expectations. Section IV offers some concluding remarks.

II. CIRCUIT

A. General remarks

Figure 1 shows a schematic diagram of the circuit used to model Eq. (1). The circuit has a modular design and may, with small changes, be used to study any of several different chaotic systems, each corresponding to a different nonlinear function $D(x)$.[16,17] The variable resistor R_v acts as a control parameter, moving the system in and out of chaos, and the input voltage V_0 may be either positive or negative.[26] All unlabeled resistors (capacitors) have the same nominal resistance R (capacitance C). The box labeled $D(x)$ in Fig. 1 represents the nonlinearity in the circuit, which is necessary

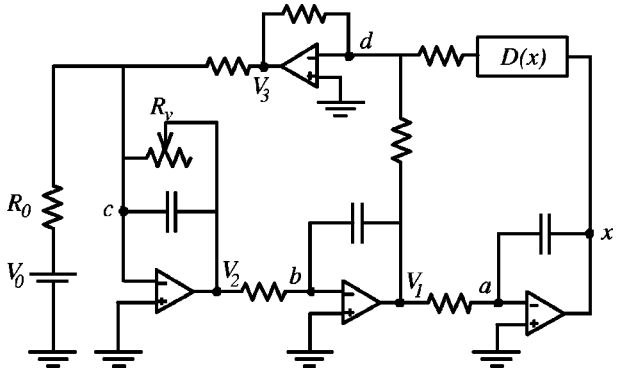

Fig. 1. Schematic diagram of the circuit described by Eq. (6). The box labeled $D(x)$ represents a nonlinear subcircuit. Nominal values for the unlabeled resistors and capacitors are $R=47\ \mathrm{k}\Omega$ and $C=1\ \mu\mathrm{F}$. Approximate values for the input voltage and resistor are $V_0=0.250$ V and $R_0=157\ \mathrm{k}\Omega$. Also, $V_1=-\dot{x}$ and $V_2=\ddot{x}$. The experiment employs dual LMC6062 operational amplifiers, chosen for their high input impedance. Power supplies for the operational amplifiers are tied capacitively to ground to reduce the effects of noise on the circuit.

for the circuit to exhibit chaotic behavior. The voltage at the output of the box (on the left) is related to that at its input by the functional relation $V_{\mathrm{out}}=D(V_{\mathrm{in}})$.

The circuit in Fig. 1 contains three successive inverting integrators with outputs at the nodes labeled V_2, V_1, and x, as well as a summing amplifier with its output at V_3. If we use Kirchhoff's rules at nodes a-d (along with the "golden rules" for op amps[27]), we obtain the following relations among the voltages:[28]

$$V_1=-RC\frac{dx}{dt}=-\dot{x}, \tag{2}$$

$$V_2=-RC\frac{dV_1}{dt}=\ddot{x}, \tag{3}$$

$$RC\frac{dV_2}{dt}=-\left(\frac{R}{R_v}\right)V_2-\left(\frac{R}{R_0}\right)V_0-V_3, \tag{4}$$

$$V_3=-V_1-D(x), \tag{5}$$

where the dots denote derivatives with respect to the dimensionless variable $\tilde{t}=t/(RC)$. The substitution of Eqs. (2), (3), and (5) into Eq. (4) yields

$$\dddot{x}=-\left(\frac{R}{R_v}\right)\ddot{x}-\dot{x}+D(x)-\left(\frac{R}{R_0}\right)V_0. \tag{6}$$

Equation (6) may be compared with Eq. (1). It is straightforward to generalize Eq. (6) to the case where the resistors and capacitors differ slightly from their nominal values.

In Ref. 17 the nonlinearity in the circuit was taken to have the form of an absolute value, $D(x)=|x|$. The solutions of the differential equation corresponding to this form become unbounded when R_v exceeds a certain threshold. In the circuit itself, such unbounded solutions manifest themselves through saturated op amps, making the circuit somewhat difficult to work with. In particular, it was found that certain power supplies to the circuit had to be turned on in a specific order and in quick succession or the circuit would saturate. This instability manifested itself for all values of R_v, not just those beyond the threshold.

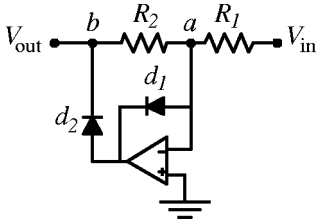

Fig. 2. Schematic diagram of the subcircuit in the box in Fig. 1. The relation between the output and input voltages is given by $V_{\mathrm{out}}=D(V_{\mathrm{in}})=-(R_2/R_1)\min(V_{\mathrm{in}},0)$.

In the present work we employ a different nonlinear subcircuit than in Ref. 17. The nonlinearity used here models the function $D(x)=-6\min(x,0)$ and does not lead to unbounded solutions. The resulting circuit is generally much more stable to work with, making it ideal for use with undergraduate students and for other applications.

Figure 2 shows the nonlinear subcircuit used in this work to model the function $D(x)$ noted above. Slight variations of this circuit[27] are used widely in various electronic applications such as AC voltmeters. To show that the circuit yields the desired functional form, we use the Shockley equation to model the $I-V$ curves for the diodes,

$$I_D=I_S(e^{\alpha V_D}-1), \tag{7}$$

where I_D and V_D represent the current through and voltage across each diode, respectively. For the BAV20 silicon diodes that we use, the reverse bias current I_S is of order a few nA and α is of order $20\ \mathrm{V}^{-1}$. If we employ Kirchhoff's rules at nodes a and b in Fig. 2, we obtain the following transcendental equation relating the input and output voltages in Fig. 2:[29]

$$V_{\mathrm{out}}+\frac{1}{\alpha_2}\ln\left[1+\frac{V_{\mathrm{out}}}{I_{S_2}R_2}\right]=-\frac{1}{\alpha_1}\ln\left[1+\frac{1}{I_{S_1}}\left(\frac{V_{\mathrm{in}}}{R_1}+\frac{V_{\mathrm{out}}}{R_2}\right)\right]. \tag{8}$$

We take $\alpha_1\sim\alpha_2\sim 20\ \mathrm{V}^{-1}$, $I_{S_1}\sim I_{S_2}\sim 3$ nA and resistances of the order 10 kΩ and find that the solution of Eq. (8) is very well represented by the approximate expression

$$V_{\mathrm{out}}=D(V_{\mathrm{in}})=-\left(\frac{R_2}{R_1}\right)\min(V_{\mathrm{in}},0). \tag{9}$$

In the experiment we choose R_1 and R_2 such that $R_2/R_1\approx 6$. In this case the exact solution of Eq. (8) gives voltages of order -10^{-4} V (instead of zero) for positive input voltages. For negative input voltages the exact solution of Eq. (8) differs from the approximation in Eq. (9) by an amount of order $-I_SR_2\sim -2\times 10^{-4}$ V. This amount would yield a 0.3% correction when $V_{\mathrm{in}}=-0.01$ V and a 0.03% correction when $V_{\mathrm{in}}=-0.1$ V. Figure 3 shows an experimental measurement of $D(x)$ as a function of x, with the fit in Eq. (9) superimposed on the data, demonstrating that Eq. (9) models the subcircuit quite well.

One interesting feature that we have observed with the subcircuit is that extremely intense light tends to decrease the output voltage somewhat. (The casing on the diodes is evidently not completely opaque.) No significant effects were observed with normal ambient room light.

The important point expressed in Eq. (9) and the ensuing discussion is that the op amps in Fig. 2 drive the diodes in

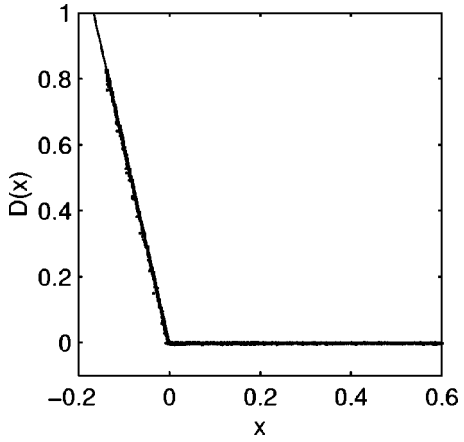

Fig. 3. Experimental measurement of the function $D(x)$ for the nonlinear subcircuit shown in Fig. 2. The superimposed line shows the function defined in Eq. (9). Both x and $D(x)$ are in volts.

such a way that the circuit becomes quite insensitive to the particular characteristics of the diodes themselves, that is, to a very good approximation the solution of Eq. (8) does not depend on α or I_S. A related but slightly simpler version of the circuit in Figs. 1 and 2 employs a bare diode to model the function $\min(x,0)$.[15] A detailed comparison between theory and experiment in that case involves the solution of a differential equation similar to Eq. (6), but with a function $D(x)$ that contains a gradual ''knee'' rather than a sharp discontinuity in slope. The numerical results depend very sensitively on the exact shape of the knee, so that one must perform a very careful measurement of the diode's $I-V$ curve, and then solve a transcendental equation to determine $D(x)$ accurately.[30] In contrast, the nonlinearity in the present circuit is very well described by the simple piecewise linear function in Eq. (9), which requires no special handling and yields a very accurate representation of the experimental results.

B. Technical details

A few details have been omitted from Fig. 1 for the sake of clarity. In the first place, the circuit is ''floated'' at a false ground of approximately 0.725 V to accommodate various digital elements in the circuit that were added to collect a time series record of the signal. (These digital elements require voltages to be in the range 0–5 V.) Furthermore, the variable resistor shown in Fig. 1 is actually composed of a 46.3 kΩ fixed resistor in series with eight 256-step DS1803 digital potentiometers (each of nominal resistance $\sim 10\ \mathrm{k}\Omega$). Also omitted from Fig. 1 are simple amplification circuits at the nodes corresponding to x and $-\dot{x}$, which are used to make more efficient use of the 0–5 V range available for analog-to-digital (A/D) measurements.

The digital potentiometers and fixed resistor that comprise R_v in Fig. 1 yield approximately 2000-step resolution over the range from about 50 kΩ to about 130 kΩ. This resolution allows for a very detailed bifurcation plot (see Fig. 4) and also lets the user find very narrow windows of periodicity within bands of chaotic behavior. The digital potentiometers are mildly nonlinear devices in the sense that the resistance of a given potentiometer depends on the voltages at its low and wiper leads. To minimize the effect of this nonlinearity, we calibrate the potentiometers near 0.725 V, the floating ground for the experiment. The potentiometers themselves are controlled digitally by a PIC16773 microcontroller, which also is used to measure the voltages at the nodes corresponding to x and $-\dot{x}$. These voltage measurements are made at a frequency of 166.7 Hz and are stored temporarily on an AT24C256 EEPROM before being transferred serially to a personal computer to be written to a file. Data collection over the entire range of interest takes approximately 12 hours. At present, the limiting factor is the time required to store data on the EEPROM. Modifications are currently planned that will significantly improve this aspect of the experiment.[31]

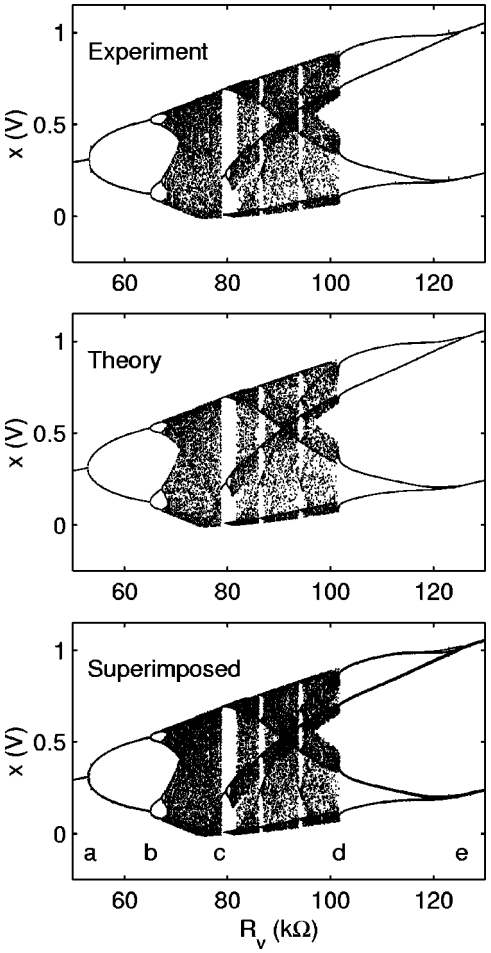

Fig. 4. Experimental, theoretical, and superimposed bifurcation plots for the circuit in Figs. 1 and 2.

III. RESULTS

A. Bifurcation plot

Figure 4 shows experimental and theoretical plots of local maxima of x as a function of R_v. For $R_v \lesssim 53\ \mathrm{k}\Omega$ the voltage varies periodically, with a single maximum occurring near 0.3 V. Near 53 kΩ there is a bifurcation to a period-two wave form. In this case the signal goes through two local maxima before repeating. The signal continues to follow a period-doubling route to chaos as R_v is increased, finally becoming chaotic near 68 kΩ. In chaotic regions the signal never repeats itself, that is, the period is infinite. Also evident in the plots are several windows of periodicity between

Table I. Comparison of theoretical and experimental bifurcation points. The labels a–e are indicated in the bottom plot in Fig. 4.

	Expt. (kΩ)	Theory (kΩ)	Diff. (kΩ)	Diff. (%)
a	53.2	52.9	0.3	0.6
b	65.0	65.0	0.0	0.0
c	78.8	78.7	0.1	0.1
d	101.7	101.7	0.0	0.0
e	125.2	125.5	−0.3	−0.2

bands of chaos. Most of the experimentally observed periodic windows are quite narrow, and can include high-period orbits. (See, for example, the period-10 orbit in Fig. 7, which comes from a periodic window of width 0.3 kΩ near $R_v = 98.2\ \mathrm{k}\Omega$.)

The top plot in Fig. 4 shows the experimental maxima. To reduce the effects of noise on this plot, a cubic polynomial is fit to points surrounding possible maxima. Spurious maxima are removed using various cuts. The fitting procedure generally works very well, but tends to underestimate maxima by up to about 6 mV. The middle plot shows the theoretical bifurcation plot obtained by solving Eq. (6) with the nonlinearity in Eq. (9). The numerical solution is obtained using a fourth-order Runge–Kutta algorithm with a fixed step size corresponding to 0.125 ms. Measured (rather than nominal) values for the resistors and capacitors are used in the numerical work. The bottom plot shows the experimental and theoretical plots superimposed and demonstrates the excellent agreement between the two plots. This agreement also is shown in Table I, which compares the locations of several bifurcation points. The bifurcation points all agree to within 1%. The excellent agreement between theory and experiment is due in large part to the nearly ideal behavior of the nonlinear subcircuit. If a single diode is used to approximate the function in Eq. (9), the agreement between theory and experiment is noticeably poorer (even if one attempts to model the $I-V$ characteristics of the diode carefully.) Figure 5 shows an expanded view of a section of the experimental bifurcation plot shown in Fig. 4, showing the fine detail obtained in the experiment.

B. Power spectral densities and phase portraits

Figure 6 contains several experimental power spectra and illustrates the period-doubling route to chaos followed by the system as R_v is increased from approximately 51 kΩ to 72 kΩ. In each case the results are obtained from an 8192-point fast Fourier transform (FFT) of the corresponding experimental x values.[32] The uppermost plot shows an example of period-one behavior and contains a strong peak at the dominant frequency of approximately 3.1 Hz. The harmonic peaks occurring at integer multiples of the dominant frequency indicate, as would be expected, that the oscillations are not perfectly sinusoidal. A strong peak near 3 Hz is evident in each of the other plots as well, although the peak moves to higher frequencies as R_v increases. The period-one case also contains a theoretical curve for comparison.[33] The agreement between theory and experiment is excellent, with the positions of the peaks agreeing to within one percent. This level of agreement between theory and experiment is found for other values of R_v as well. The second plot in Fig. 6 shows an example of period-two behavior. In this case the oscillating voltage (shown in the inset) passes through two different maxima before repeating. The spectral density plot contains a new peak at half the dominant frequency, illustrating the fact that period doubling is equivalent to frequency halving. The trend is continued in the third plot, which shows an example of a period-four case. The bottom plot shows the power spectrum for a chaotic case. Despite the noisy appearance of the spectrum, there is still a strong peak near 3.4 Hz.

Several experimental phase portraits are shown in Fig. 7. In each case x and $\dot{x}$ are determined experimentally from the

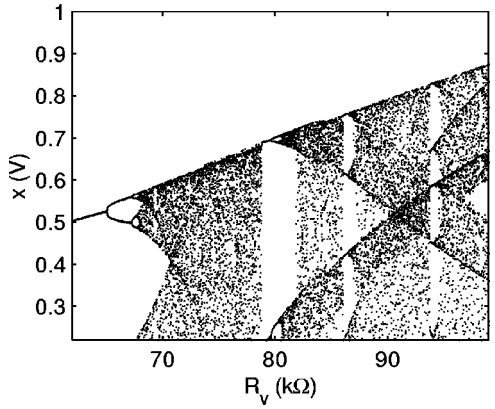

Fig. 5. An expanded view of part of the experimental bifurcation plot shown in Fig. 4.

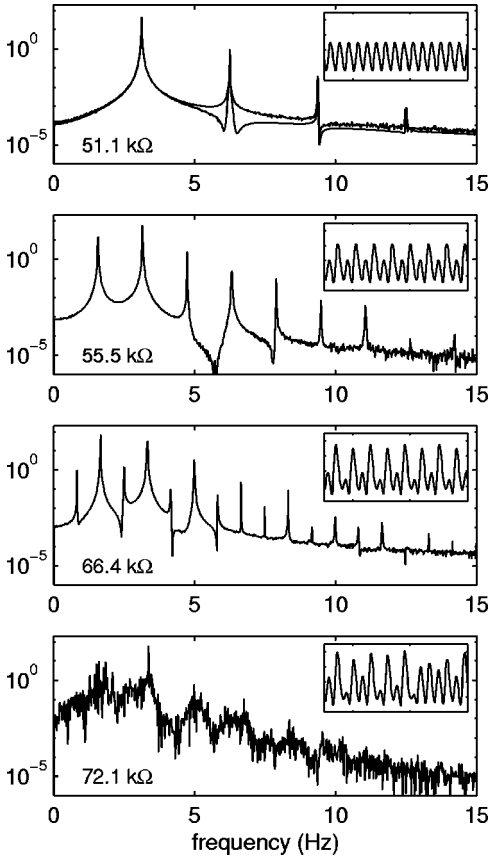

Fig. 6. Experimental power spectral density plots showing the period-doubling route to chaos as R_v is increased. The value of R_v is indicated in the lower left corner. The inset in each plot shows a sample of the experimental time series data used to generate the corresponding spectral density. The smoother line in the period-one plot shows the theoretical spectral density.

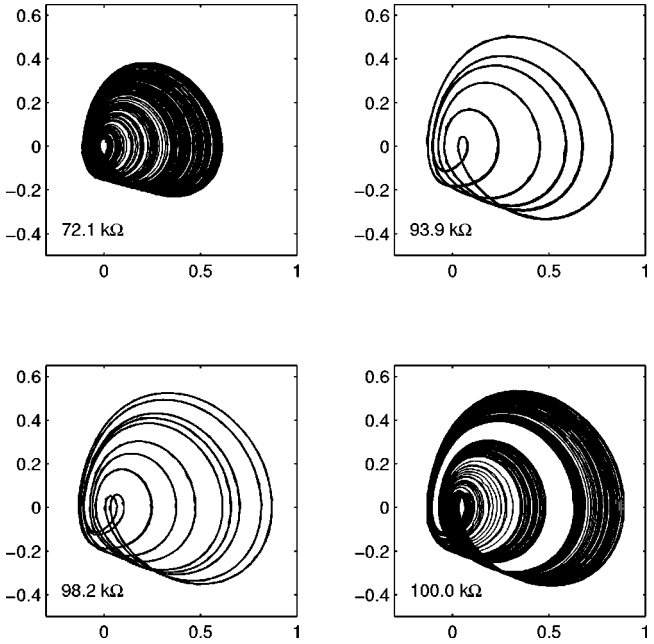

Fig. 7. Experimental phase portraits for several different values of the variable resistance R_v. In each plot x and $\dot{x}$ are plotted (in volts) on the horizontal and vertical axes, respectively. A theoretical curve is superimposed on the period-six case for comparison, although the curve is not distinguishable from the experimental curve. The period-10 attractor comes from a narrow window that is barely discernible at the far right edge of Fig. 5.

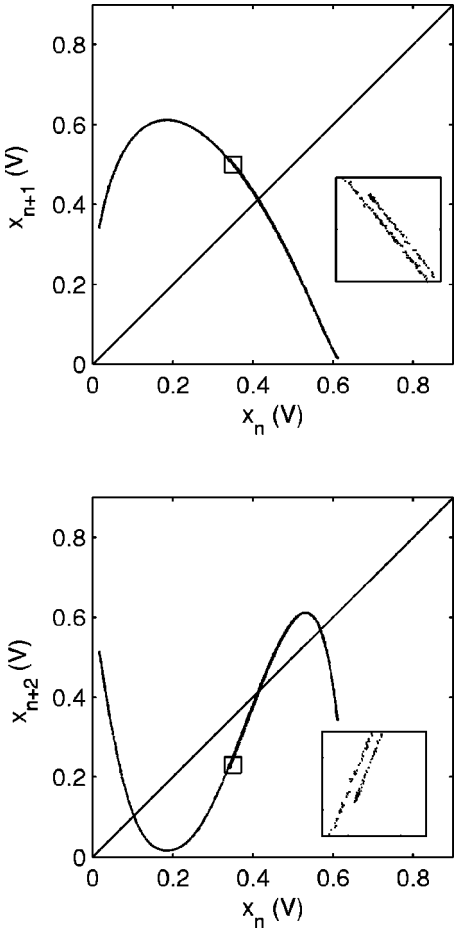

Fig. 9. First- and second-return maps for $R_v = 72.1\ \mathrm{k}\Omega$, taken from experimental data. The insets are magnified by a factor of approximately 6.5 and show the fractal structure of the plots. The intersections of the return maps with the diagonal lines give evidence for (unstable) period-one and -two orbits in the data sets. Such orbits do indeed exist, as seen in Fig. 10.

appropriate nodes in the circuit. The upper-left and lower-right plots show two different chaotic attractors. The latter is a two-banded attractor taken from the region just to the left of the final bifurcation out of chaos in Fig. 4. The upper-right and lower-left plots show period-six and -10 attractors, which are taken from relatively narrow windows of periodicity discernible in Figs. 4 and 5. A theoretical curve is superimposed on the period-six attractor, but is not distinguishable due to the excellent agreement. Comparisons between theoretical and experimental phase portraits for several periodic attractors show agreement typically within 3–6 mV, with the agreement being somewhat worse for larger values of R_v. For $R_v = 123.2\ \mathrm{k}\Omega$ (near the bifurcation from period-four to period-two) the theoretical and experimental attractors differ by up to about 8 mV. Figure 8 shows a stereoscopic plot of the first 2000 points of one of the chaotic attractors in Fig. 7.

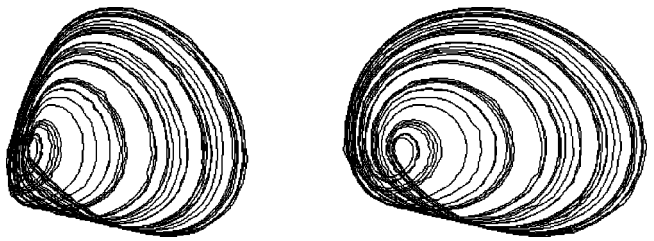

Fig. 8. Stereoscopic plot of the chaotic attractor at $R_v = 72.1\ \mathrm{k}\Omega$. The x and $\dot{x}$ coordinates are taken from experimental data. The third coordinate is proportional to $\ddot{x}$ and is determined numerically by using pairs of $\dot{x}$ values.

C. Case study of a chaotic attractor

In this section we focus our attention on the chaotic attractor near $R_v = 72.1\ \mathrm{k}\Omega$. Phase portraits for this attractor are shown in Figs. 7 and 8. One point of comparison between theory and experiment for this case is provided by the return map associated with the attractor. To construct a return map for a time-continuous system, we first construct an array containing successive maxima x_n. The r-return map is then a plot of x_{n+r} versus x_n. For a system such as ours, the return maps have a fractal structure. Figure 9 shows experimental plots of the first- and second-return maps for $R_v = 72.1\ \mathrm{k}\Omega$. The inset in each case shows the first splitting of the return map associated with its fractal structure. Subsequent splittings at higher magnification are not observable experimentally due to noise in the experimental data. A comparison with the theoretical first-return map shows quite good agreement, with the theoretical values typically being larger than the experimental ones by 2–4 mV. The disagreement is due in part to the fact that our fitting procedure for determining experimental maxima tends to underestimate the maxima slightly. The theoretical first-return map shows further fractal structure. For example, a numerical solution with step size 0.015 625 ms reveals that the main inverted parabola of the return map is actually two separate lines, sepa-

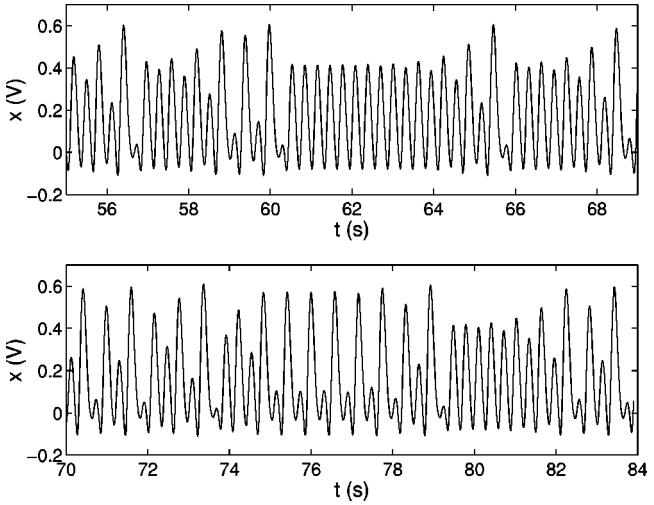

Fig. 10. Experimental wave forms showing unstable period-one and -two orbits within the chaotic time series data for $R_v = 72.1\ \mathrm{k}\Omega$. The top plot shows an unstable period-one orbit starting shortly after $t = 60$ s, with a maximum near 0.41 V. The bottom plot shows an unstable period-two orbit starting just before $t = 75$ s, with maxima near 0.57 V and 0.10 V. The plots themselves are taken from different datasets.

rated by about 0.026 mV at the peak (further splitting of these lines is not evident with this step size). The experimental noise at the peak has a width of about 1 mV, explaining why the splitting is not observed experimentally.

Return maps can be used to study periodic orbits within the data set.[34,35] A diagonal line is superimposed on each of the plots in Fig. 9. In the top plot the diagonal intersects the first-return map near $x_n \simeq 0.41$ V, giving evidence for a period-one orbit within the data set. Because the magnitude of the slope of the return map is greater than unity at that point, the period-one orbit is unstable.[36] A search through the experimental time series data does indeed yield unstable period-one orbits within the chaotic oscillations. The top plot in Fig. 10 shows such an example. In this case the unstable period-one behavior persists for approximately 10 oscillations (which is longer than typical for such orbits in the data set). As expected, the maxima of the oscillations occur at approximately 0.41 V. In a similar way, the intersection of the diagonal line with the second-return map in Fig. 9 gives evidence for unstable period-two orbits with maxima at approximately 0.57 V and 0.10 V. Examination of the time series data again yields such orbits, as shown in Fig. 10.

Another point of comparison between theory and experiment is the largest Lyapunov exponent, which measures the average exponential rate of spreading of nearby trajectories and is positive for a chaotic system. The experimental value of this exponent is estimated using the method of Wolf *et al.*[37] as implemented in the Chaos Data Analyzer program.[38] The time series consists of 3228 points sampled at the local maximum of each cycle for the case shown in Fig. 9. Candidate pairs are chosen assuming a noise floor of 0.1% and followed for one cycle. The resulting largest Lyapunov exponent (base e) is estimated to be $1.34 \pm 0.08\ \mathrm{s}^{-1}$. By comparison, iterating the theoretical expression in Eqs. (6) and (9) (modified slightly to use the measured component values) gives a spectrum of exponents[39] $(1.269, 0, -15.037) \pm 0.001\ \mathrm{s}^{-1}$, in agreement within the estimated errors of about 6%. From these values, the Kaplan–Yorke dimension[40] is found to be $D_{\mathrm{KY}} = 2 + 1.269/15.037 \simeq 2.084$. The proximity of this value to two explains why the return map is a relatively thin fractal.

IV. DISCUSSION AND CONCLUSIONS

The circuit described in this work is modeled very accurately by a simple, third-order differential equation whose solutions display a rich variety of chaotic and periodic behavior. Investigation of the circuit yields excellent agreement between theory and experiment for quantities such as power spectra, bifurcation points, phase portraits, and Lyapunov exponents. For some of these quantities the agreement is within 1%. The quality of this agreement and the stability of the circuit itself give the circuit great potential as a serious research tool for studies of synchronization, chaos control, higher-dimensional chaos, and other topics within nonlinear dynamics.

Investigation of the circuit is very accessible to undergraduates and is particularly well suited as a research project for junior- or senior-level students. The range of projects associated with the system need only be limited by the students' imaginations. A detailed investigation may be undertaken using commercially available A/D systems, or, at a somewhat less sophisticated level, the data may be digitized using a digital oscilloscope. Several options for investigation also are available without digitizing the data. For example, the $X-Y$ setting on an oscilloscope may be used to display phase portraits in real time. The circuit also may be simplified by substituting an analog potentiometer for the digital ones that we use.

Students will invariably be fascinated as they observe the changes in behavior as R_v is varied. Other variations on the circuit are also possible. For example, different nonlinearities $D(x)$ may be substituted in place of the one used here.[16,17] Furthermore, the operating frequency of the circuit (approximately $1/(2\pi RC)$) may easily be scaled by using different resistors or capacitors than those that we used. Scaling the frequency to the audio range and connecting the output to a speaker allows for an audible demonstration of chaos, with clearly distinguishable period doublings (frequency halvings) en route to chaos.[15] On the theoretical side, modeling the behavior of the circuit serves as an excellent review of differential equations for students. They might write their own programs to solve the equations or use software such as Matlab or Mathematica to do this. The circuit offers many possibilities for theoretical and experimental investigation, ranging from simple qualitative demonstrations to indepth analyses, making it ideal for use in an undergraduate setting.

ACKNOWLEDGMENTS

We thank J. Goldberg, W. Holmes, H. Voss, S. Brandle, T. Klein, J. Kolb, S. Price, K. Knapp, D. Simons, J. Oehrig, and J. Schea for valuable assistance at various stages of this work. K.K. was supported by an award from Research Corporation during early stages of this work.

[a]Electronic mail: knkiers@tayloru.edu
[b]Electronic mail: Dory_Schmidt/rad@di.mdacc.tmc.edu
[c]Electronic mail: sprott@physics.wisc.edu

[1]T. Mishina, T. Kohmoto, and T. Hashi, "Simple electronic circuit for the demonstration of chaotic phenomena," Am. J. Phys. **53**, 332–334 (1985).
[2]K. Briggs, "Simple experiments in chaotic dynamics," Am. J. Phys. **55**, 1083–1089 (1987).

[3]R. Zimmerman, S. Celaschi, and L. G. Neto, ''The electronic bouncing ball,'' Am. J. Phys. **60**, 370–375 (1992).
[4]T. Mitchell and P. B. Siegel, ''A simple setup to observe attractors in phase space,'' Am. J. Phys. **61**, 855–856 (1993).
[5]M. T. Levinsen, ''The chaotic oscilloscope,'' Am. J. Phys. **61**, 155–165 (1993).
[6]B. K. Clark, R. F. Martin, Jr., R. J. Moore, and K. E. Jesse, ''Fractal dimension of the strange attractor of the bouncing ball circuit,'' Am. J. Phys. **63**, 157–163 (1995).
[7]B. K. Jones and G. Trefan, ''The Duffing oscillator: A precise electronic analog chaos demonstrator for the undergraduate laboratory,'' Am. J. Phys. **69**, 464–469 (2001).
[8]P. K. Roy and A. Basuray, ''A high frequency chaotic signal generator: A demonstration experiment,'' Am. J. Phys. **71**, 34–37 (2003).
[9]T. Matsumoto, L. O. Chua, and M. Komuro, ''The double scroll,'' IEEE Trans. Circuits Syst. **32**, 797–818 (1985).
[10]T. Matsumoto, L. O. Chua, and M. Komuro, ''Birth and death of the double scroll,'' Physica D **24**, 97–124 (1987).
[11]G. Chen and T. Ueta, editors, *Chaos in Circuits and Systems* (World Scientific, London, 2002).
[12]T. P. Weldon, ''An inductorless double scroll chaotic circuit,'' Am. J. Phys. **58**, 936–941 (1990).
[13]A. S. Elwakil and M. P. Kennedy, ''Generic RC realizations of Chua's circuit,'' Int. J. Bifurcation Chaos Appl. Sci. Eng. **10**, 1981–1985 (2000).
[14]A. S. Elwakil and M. P. Kennedy, ''Construction of classes of circuit-independent chaotic oscillators using passive-only nonlinear devices,'' IEEE Trans. Circuits Syst., I: Fundam. Theory Appl. **48**, 289–307 (2001).
[15]J. C. Sprott, ''Simple chaotic systems and circuits,'' Am. J. Phys. **68**, 758–763 (2000).
[16]J. C. Sprott, ''A new class of chaotic circuit,'' Phys. Lett. A **266**, 19–23 (2000).
[17]K. Kiers, T. Klein, J. Kolb, S. Price, and J. C. Sprott, ''Chaos in a nonlinear analog computer,'' Int. J Bifurcations Chaos (to be published).
[18]H. P. W. Gottlieb, ''Question #38. What is the simplest jerk function that gives chaos?,'' Am. J. Phys. **64**, 525 (1996).
[19]S. J. Linz, ''Nonlinear dynamical models and jerky motion,'' Am. J. Phys. **65**, 523–526 (1997).
[20]J. C. Sprott, ''Some simple chaotic jerk functions,'' Am. J. Phys. **65**, 537–543 (1997).
[21]S. J. Linz and J. C. Sprott, ''Elementary chaotic flow,'' Phys. Lett. A **259**, 240–245 (1999).
[22]J. C. Sprott and S. J. Linz, ''Algebraically simple chaotic flows,'' Int. J. Chaos Theory Appl. **5**, 3–22 (2000).
[23]E.-W. Bai, K. E. Lonngren, and J. C. Sprott, ''On the synchronization of a class of electronic circuits that exhibit chaos,'' Chaos, Solitons Fractals **13**, 1515–1521 (2002).
[24]K. M. Cuomo and A. V. Oppenheim, ''Circuit implementation of synchronized chaos with applications to communications,'' Phys. Rev. Lett. **71**, 65–68 (1993).
[25]The circuit also differs from that in Ref. 15 in a few other respects. For example, the present circuit does not use a passive integrator.
[26]For the particular circuit that we study only the combination V_0R/R_0 is relevant, and it only affects the amplitude of the signal (as long as the op amps do not saturate). Thus V_0 cannot be used as a control parameter for this circuit. Such is not necessarily the case if different nonlinearities are employed.
[27]P. Horowitz and W. Hill, *The Art of Electronics*, 2nd ed. (Cambridge University Press, New York, 1989).
[28]Note that because the output of an integrator is the integral of its input, its input is also the derivative of its output.
[29]Note that this expression assumes that zero current leaves the output, a situation that holds more rigorously if the output is followed by a voltage follower amplifier. We do not use a voltage follower in the experiment. As a result, Eq. (8) is slightly altered once the subcircuit is inserted into the circuit itself, with the factor $1/R_2$ on the left-hand side replaced by $1/R_2 + 1/R$. The approximation quoted in Eq. (9) is not affected by this change.
[30]In a detailed study of the simpler single-diode circuit of Ref. 15, we employed a piecewise fit of the diode's $I-V$ curve (using several values of α and I_S). Even with the careful fit to the $I-V$ curve, the agreement between theoretical and experimental bifurcation points was not as good as in the present case, and the theoretical and experimental bifurcation diagrams contained some noticeable qualitative differences.
[31]http://www.css.tayloru.edu/~knkiers
[32]Note that the data set is AC-coupled before the FFT to eliminate a strong peak near zero Hz.
[33]One might expect the theoretical curve to contain a series of delta functions. The finite sample size (8192 points) leads to the observed nonzero widths of the peaks in this curve.
[34]D. P. Lathrop and E. J. Kostelich, ''Characterization of an experimental strange attractor by periodic orbits,'' Phys. Rev. A **40**, 4028–4031 (1989).
[35]C. Flynn and N. Wilson, ''A simple method for controlling chaos,'' Am. J. Phys. **66**, 730–735 (1998).
[36]E. Ott, *Chaos in Dynamical Systems* (Cambridge University Press, New York, 1993).
[37]A. Wolf, J. B. Swift, H. L. Swinney, and J. A. Vastano, ''Determining Lyapunov exponents from a time series,'' Physica D **16**, 285–317 (1985).
[38]J. C. Sprott and G. Rowlands, *Chaos Data Analyzer: The Professional Version* (Physics Academic Software, Raleigh, NC, 1995).
[39]J. C. Sprott, *Chaos and Time-Series Analysis* (Oxford University Press, Oxford, 2003).
[40]J. Kaplan and J. Yorke, in *Lecture Notes in Mathematics*, edited by H.-O. Peitgen and H.-O. Walther (Springer, Berlin, 1979), Vol. 370, pp. 228–237.

Proportional feedback control of chaos in a simple electronic oscillator

Richard J. Wiener,[a] Kristine E. Callan, and Stephen C. Hall
Department of Physics, Pacific University, Forest Grove, Oregon 97116

Thomas Olsen
Department of Physics, Lewis & Clark College, Portland, Oregon 97219

(Received 10 July 2005; accepted 16 December 2005)

We demonstrate the control of chaos in a nonlinear circuit constructed from readily available electronic components. Control is achieved using recursive proportional feedback, which is applicable to chaotic dynamics in highly dissipative systems and can be implemented using experimental data in the absence of model equations. The application of recursive proportional feedback to a simple electronic oscillator provides an undergraduate laboratory problem for exploring proportional feedback algorithms used to control chaos.
[DOI: 10.1119/1.2166367]

I. INTRODUCTION

Chaos theory is the study of deterministic systems whose dynamics are aperiodic and depend sensitively on initial conditions.[1] Chaotic systems have long term behavior that is unpredictable. Nonlinear dynamical systems often behave chaotically for certain ranges of system parameters; for other parameter ranges they behave periodically and thus predictably. Proportional feedback control of chaos involves perturbing a system parameter, while maintaining its value within its normally chaotic range, to achieve stabilization of a selected trajectory on the system's chaotic attractor. In this paper we focus on a proportional feedback control strategy that stabilizes periodic dynamics.

In 1990, Ott, Grebogi, and Yorke (OGY)[2] introduced a proportional feedback algorithm suitable for a large class of nonlinear oscillators. Their approach employs a feedback loop that applies small perturbations to a system at the end of each oscillation, with each perturbation proportional to the difference between the current state and a desired state. This strategy is an extension of engineering control theory.[3,4] The OGY algorithm precipitated an outpouring of experimental and theoretical work on controlling chaotic dynamics.[5] Proportional feedback control has been demonstrated for a wide variety of dynamical systems including mechanical,[6,7] fluid,[8] electronic,[9] optical,[10] chemical,[11,12] and biological[13] systems. Control via proportional feedback is now a central topic of research in nonlinear dynamics and has been extended experimentally to chaotic spatial patterns.[14,15] Given its currency and prominence, it is desirable to introduce this topic in undergraduate courses on chaos.

Baker[16] has provided a clear presentation of the OGY algorithm. However, the algorithm is challenging to implement experimentally because it requires sampling more than one dynamical variable in real time. Dressler and Nitsche[17] showed that the OGY algorithm can be modified to allow for measurements of a single dynamical variable. But there are much simpler alternatives to the OGY algorithm for highly dissipative systems, that is, systems whose dynamics can be reduced to one-dimensional (1D) return maps. For this special but not uncommon case, Peng, Petrov, and Showalter[18] introduced simple proportional feedback, and Rollins, Parmananda, and Sherard[19] derived recursive proportional feedback. These less complicated proportional-feedback algorithms illustrate key ideas of control and are considerably less mathematically demanding than the OGY algorithm, which is applicable to a wider range of systems.

In this paper we present a derivation of recursive proportional feedback at a level suitable for an introductory course on chaos, and we explain why recursive proportional feedback is more generally applicable than simple proportional feedback. Flynn and Wilson[20] and Corron, Pethel, and Hopper[21] have presented other simple methods of controlling chaos that are also suitable for introducing undergraduates to this topic. However, a discussion of simple proportional feedback and recursive proportional feedback allows us to address the issues of the stability and the range of applicability of individual control algorithms.

Recently, Kiers, Schmidt, and Sprott (KSS)[22] introduced a simple nonlinear electronic circuit that can be used to study chaotic phenomena. This circuit employs readily available electronic components and is well-suited for advanced undergraduate instructional laboratories. A novel feature of the KSS circuit is the presence of an almost ideal nonlinear element, which results in excellent agreement between the experimental circuit and numerical solutions of the differential equation that models the dynamics of the circuit. The circuit allows for precise measurements of bifurcation diagrams, phase portraits, return maps, power spectra, Lyapunov exponents, and the fractal dimension of chaotic attractors. A further advantage of using the KSS circuit for undergraduate experiments is that the time scale can be adjusted so that the periods of oscillation are on the order of a second, making the circuit an ultra-low-frequency electronic oscillator. Students can observe the dynamics in real time, and there is sufficient time during the oscillations for a digital processor to compute the requisite perturbations for chaos control. Undergraduates can readily wire the circuit, interface it to a computer-based data acquisition board, and write a program to acquire data and apply a proportional feedback loop. There are many data acquisition, output, and analysis systems in use in undergraduate laboratories that could be employed.

In this paper we show that the KSS circuit can be used to illustrate proportional feedback control of chaos by applying recursive proportional feedback to its dynamics. We show how chaos can be controlled experimentally, even in the absence of model equations, by determining the values of the coefficients in the recursive proportional feedback algorithm only from experimental data, without reference to the differ-

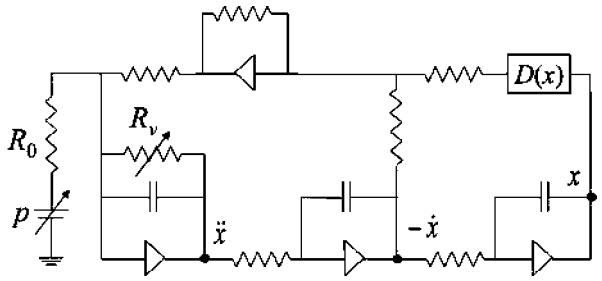

Fig. 1. Circuit diagram of the electronic oscillator modeled by Eq. (1). We used dual LMC6062 op amps, chosen for their high input impedance, throughout the circuit. The effects of noise on the circuit are reduced by capacitively tying the power supplies for the op amps to ground. The wiring into the op amps is to their inverting (−) inputs; the noninverting (+) inputs are grounded. The supply voltages for the op amps were set at ±15 V. We chose component values for which the circuit oscillates chaotically. The unmarked resistors and capacitors are $R=46.6\pm0.3$ kΩ and $C=2.29\pm0.03$ μF. The variable resistor $R_V=81.4\pm0.1$ kΩ and $R_0=156.9\pm0.1$ kΩ.

ential equation that models the dynamics of the circuit. However, because the model equation is known, an important feature of this circuit is that one can perform analytic and numerical investigations in parallel with the experiment. Our demonstration of control of a chaotic electronic oscillator fits well in an undergraduate course on nonlinear dynamics or computer interfaced experimentation.

II. CHAOS IN A SIMPLE ELECTRONIC OSCILLATOR

Jerk equations (third-order autonomous ordinary differential equations) with nonlinearities involving piecewise linear functions often can be implemented electronically using only resistors, capacitors, diodes, and op amps.[23] Many of these equations and corresponding electronic circuits exhibit chaotic oscillations for a range of system parameters. The KSS circuit is an example of such a chaotic electronic oscillator. Its diagram is shown in Fig. 1, and it can be assembled on a standard solderless breadboard. The circuit contains three successive inverting amplifiers with output voltages at the nodes labeled x, $-\dot{x}$, and $\ddot{x}$. These outputs are the dynamical variables of the system. The input voltage for the circuit, which is labeled p, is an accessible system parameter that can be varied. The box labeled $D(x)$ represents the nonlinear element in the circuit, which is necessary for chaotic oscillations.

By using Kirchhoff's rules and the golden rules for op amps, we obtain the following dynamical equation (see Ref. 22 for details):

$$\dddot{x} = -\left(\frac{R}{R_V}\right)\ddot{x} - \dot{x} + D(x) - \left(\frac{R}{R_0}\right)p, \tag{1}$$

where a dot denotes differentiation with respect to the dimensionless time scaled by RC. R_V is a variable resistor; varying R_V allows one to explore a wide range of the circuit's dynamical behavior.[22] To make explicit that there are three dynamical variables for this circuit (as well as to facilitate numerical integration using a Runge-Kutta method), we rewrite Eq. (1) as a system of three first-order autonomous ordinary differential equations. If we define $y \equiv \dot{x}$ and $z \equiv \ddot{x}$, then

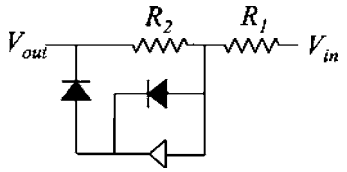

Fig. 2. The nonlinear subcircuit $D(x)$ corresponding to the box in Fig. 1. The wiring into the op amp is to its inverting (−) input; the noninverting (+) input is grounded and 1N914 diodes are used. The resistors have values $R_1=15.1\pm0.1$ kΩ and $R_2=88.9\pm0.1$ kΩ so that $R_2/R_1\approx6$.

$$\dot{x} = y, \tag{2a}$$

$$\dot{y} = z, \tag{2b}$$

$$\dot{z} = -\left(\frac{R}{R_V}\right)z - y + D(x) - \left(\frac{R}{R_0}\right)p. \tag{2c}$$

The nonlinearity in the KSS circuit is modeled by the function $D(x)=-(R_2/R_1)\min(x,0)$; Figure 2 shows the diagram for this nonlinear subcircuit. The agreement between the piecewise linear function $D(x)$ and the actual output of the subcircuit is excellent and leads to impressive agreement between measured values of the dynamical variables and numerical solutions of Eq. (2).[22]

One technique for representing chaotic dynamics is to construct return maps. For a first-iterate return map, a sequence of maximum values of a dynamical variable is used and x_{n+1} is plotted versus x_n. If this plot forms a thin, approximately 1D curve, then the dynamics have been reduced to a 1D map: $x_{n+1}=f(x_n,p_0)$, where p_0 is the value of the system parameter at which the sequence was collected. Figure 3 shows a 1D return map for the KSS circuit for a sequence of maxima of the output voltage x during chaotic oscillations. In practice there may be several other system parameters on which the mapping depends, as is the case for the KSS circuit (for example, R_V, R_0, R_1, R_2, and R). However, if these other parameters remain fixed throughout the experiment, they can be ignored. Systems that can be reduced to 1D maps are referred to as *highly dissipative*.[19] Examples of other experimental systems that exhibit highly dissipative chaotic dynamics include a gravitationally buck-

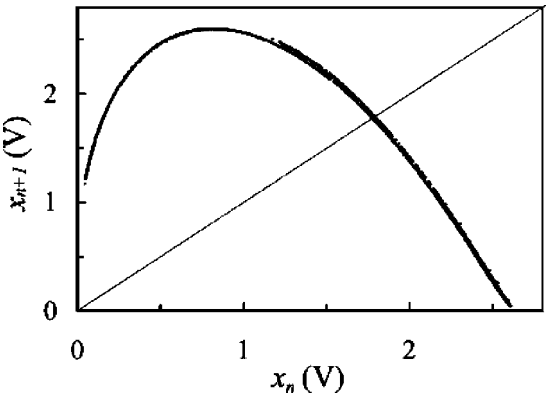

Fig. 3. First-iterate return map of an experimentally measured sequence of 1913 maxima of x, collected with the input voltage fixed at $p_0=1.0000$ V. The intersection of the map with the $x_{n+1}=x_n$ line corresponds to an unstable period-one fixed point.

led magnetoelastic ribbon,[6] Belousov-Zhabotinsky oscillating chemical reactions,[24] electrodissolution in an electrochemical cell,[11,12] electronic circuits,[25] and phase slips in a pattern of fluid vortices.[14]

III. DERIVATION OF THE PROPORTIONAL FEEDBACK CONTROL ALGORITHM

When a system is in a chaotic state, there typically are infinitely many unstable periodic orbits embedded in its dynamics. A fixed point of a return map corresponds to a periodic orbit. For example, a period-one orbit returns to the same value after one oscillation: $x_{n+1}=x_n$. Thus a period-one fixed point is defined as a value of the dynamical variable for which the map returns the same value: $x_F \equiv f(x_F, p_0)$. For systems undergoing chaotic dynamics, such fixed points are unstable, and the key to controlling chaos using proportional feedback algorithms is to stabilize a dynamical variable near an unstable fixed point. This stabilization can be accomplished by applying a sequence of small perturbations δp_n, one after each iteration of the map, to an accessible system parameter p on which the map depends. The strength of the applied perturbation is proportional to the difference between the current value of a dynamical variable and the predetermined fixed point: $\delta p_n \propto (x_n - x_F)$. The perturbations are limited in magnitude by the requirement that the adjusted parameter remain within a range for which the system is chaotic in the absence of perturbations. The control algorithm is a feedback loop that samples the variable in real time and adjusts the parameter accordingly. The carefully chosen perturbations alter the system in such a manner that the current state of the system will evolve closer to the fixed point during the next cycle of the perturbed system. This perturbing of the dynamics causes the otherwise chaotic oscillations to remain approximately periodic. To determine the proportionality constant in a control algorithm, it is necessary to identify a desired fixed point, determine how strongly unstable it is, and determine the response of the system to small changes in the parameter that will be perturbed to implement control. This procedure can be done using experimental measurements of the evolution of a single dynamical variable for various values of a system parameter prior to initiating control and requires no knowledge of an analytical model for the dynamics.

To derive the recursive proportional feedback algorithm, we consider nonlinear systems with three dynamical variables, the minimum necessary for chaos.[1] The KSS electronic oscillator is an example of such a system as can be seen from Eq. (2). For a system with three dynamical variables, x, y, and z, its chaotic attractor exists in a 3D phase space. If high dissipation limits the chaotic attractor to a very thin, nearly 2D surface, the dynamics are reducible to a 1D return map. This reduction is possible because the points on the 2D surface which intersect a particular surface of section, for example, the $y=y_c$ plane (where y_c is a constant), form a 1D curve. We may view the evolution of the system as a mapping from $(x_n, y_c, z_n) \rightarrow (x_{n+1}, y_c, z_{n+1})$ each time the phase space trajectory pierces the surface of section in the same direction. For the KSS circuit, constructing a return map using a sequence of maxima of x corresponds to selecting the $y \equiv \dot{x}=0$ plane as the surface of section. The existence of the 1D curve on the surface of section implies that there is a function of the form $z_n=h(x_n, p_{n-1})$. The subscript on p indicates that the value of p may vary each time the map is iterated, because this parameter will be perturbed during chaos control.

We define $p_n \equiv p_0 + \delta p_n$ as the value of the parameter as $x_n \rightarrow x_{n+1}$ and p_0 as the constant value for which there is uncontrolled chaos. Thus the $n-1$ subscript denotes the value of p as the dynamical variable evolves from x_{n-1} to x_n. This point is important: z_n is determined by x_n based on the position of the attractor in phase space due to the value of p at the end of the nth cycle, p_{n-1}, not the value of p at the beginning of the $n+1$ cycle, p_n. The mapping between successive points on the surface of section means that x_{n+1} is determined by a function of the form $x_{n+1}=g(x_n, z_n, p_n) = g(x_n, h(x_n, p_{n-1}), p_n)$, which can be written equivalently as

$$x_{n+1} = f(x_n, p_n, p_{n-1}). \tag{3}$$

Equation (3) is the 1D return map that results from the 1D curve on the surface of section. If the parameter p is constant during the evolution of the dynamics (as it is for the map shown in Fig. 3), the return map reduces to $x_{n+1}=f(x_n, p_0)$. But during the application of perturbations, x_{n+1} may depend on both p_n and p_{n-1}.

We expand the return map to first order about the fixed point x_F for some periodic orbit at the parameter value p_0:

$$\delta x_{n+1} \approx \mu \delta x_n + \nu \delta p_n + \omega \delta p_{n-1}, \tag{4}$$

where $\delta x_n = x_n - x_F$, $\mu = \partial f / \partial x_n$, $\nu = \partial f / \partial p_n$, and $\omega = \partial f / \partial p_{n-1}$ with all derivatives evaluated at x_F and p_0. For a chaotic system $|\mu| > 1$, which means the value of δx_n grows over successive iterations of the map and the fixed point is unstable.

To control chaos, the perturbation δp_n must force the system toward the fixed point. Also, for the control algorithm to be stable, δp_n cannot grow over successive iterations. One way these conditions can be strongly satisfied is by requiring that $\delta x_{n+2}=0$ and $\delta p_{n+1}=0$. The latter requirement moves the system to the fixed point in a single control step; further control perturbations are only needed to address the motion of the system away from the fixed point due to noise. Then starting with Eq. (4), iterating it a second time, and solving both equations simultaneously for δp_n yields $\delta p_n \approx K \delta x_n + R \delta p_{n-1}$, where

$$K = -\frac{\mu^2}{(\mu\nu + \omega)}, \tag{5a}$$

$$R = -\frac{\mu\omega}{(\mu\nu + \omega)}. \tag{5b}$$

For the recursive proportional feedback algorithm, this approximation is set to an exact equality:

$$\delta p_n = K \delta x_n + R \delta p_{n-1}. \tag{6}$$

The first term on the right-hand side of Eq. (6) is proportional to the difference between the current state of the system and the fixed point, and the second term depends recursively on the previous perturbation. Derivatives of the return map for uncontrolled chaos determine the coefficients K and R used in the control feedback loop. In the broader context of control theory, one may study the entire range of values of K and R for which the system will approach periodic behavior. This procedure is well described in Ref. 3. By using control theory one can show that the fastest approach to control is

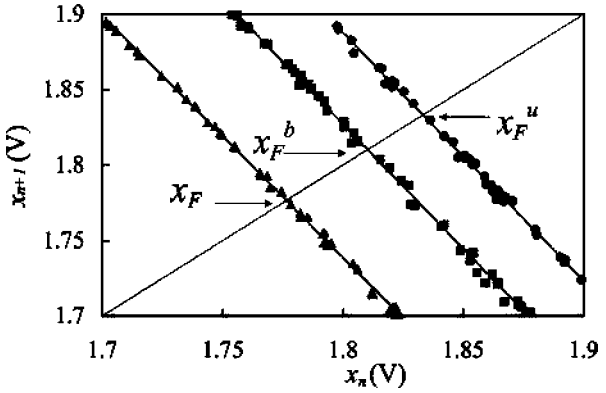

Fig. 4. The unperturbed (triangles), up (circles), and back (squares) maps near the $x_{n+1}=x_n$ line, generated experimentally according to the procedure in Sec. III with $\Delta p=0.05$ V. Linear fits to the data are also shown. The fixed points x_F, x_F^u, and x_F^b occur at the intersections of the maps and the $x_{n+1}=x_n$ line.

obtained by the choice of K and R in Eq. (5).

There is an effective experimental procedure for finding the slopes μ, ν, and ω that determine K and R. First we allow the system to run unperturbed at a constant parameter value p_0 for which the dynamics are chaotic. Then the 1D return map $x_{n+1}=f(x_n,p_0)$ is constructed and a linear fit to the map in the neighborhood of the $x_{n+1}=x_n$ line is made. The fixed point x_F is defined by the intersection of the map with the $x_{n+1}=x_n$ line,[26] and μ is the slope of the fit. To find ν and ω, it is necessary to find the dependence of the map on both p_n and p_{n-1}. This dependence is found by collecting data while repeatedly increasing the control parameter to $p_0+\Delta p$ for one oscillation and decreasing it to p_0 for the next oscillation, where Δp is a small, fixed value. Alternate pairs (x_n,x_{n+1}) of this sequence are on different return maps, designated the *up* and *back* maps. For the up map $p=p_0$ during the cycle that generates x_n and $p=p_0+\Delta p$ during the cycle that generates x_{n+1}, and conversely for the back map.[27] Fits to the up and back maps can be made and their respective fixed points, x_F^u and x_F^b, determined. Figure 4 shows the three return maps in the neighborhood of their fixed points for the KSS circuit. The shifts of the fixed points for the up and back return maps are a consequence of the changing location of the chaotic attractor in phase space as the control parameter is varied. In the neighborhood of their fixed points, each of the maps in Fig. 4 is approximately linear with slope μ:

$$f(x_n)=\mu x_n+(1-\mu)x_F, \tag{7a}$$

$$f^b(x_n)=\mu x_n+(1-\mu)x_F^b, \tag{7b}$$

$$f^u(x_n)=\mu x_n+(1-\mu)x_F^u. \tag{7c}$$

The derivatives ν and ω can be approximated by

$$\nu\approx\frac{f^u(x_F)-f(x_F)}{\Delta p}=(1-\mu)\frac{x_F^u-x_F}{\Delta p}, \tag{8a}$$

$$\omega\approx\frac{f^b(x_F)-f(x_F)}{\Delta p}=(1-\mu)\frac{x_F^b-x_F}{\Delta p}. \tag{8b}$$

Thus μ, ν, and ω, which determine the coefficients in the recursive proportional feedback algorithm, are found from the unperturbed, up, and back maps, which are constructed solely from experimental measurements of the output voltage x.

Note that if $x_F^b=x_F$, then $\omega=0$ and the recursive term in Eq. (6) goes to zero, which means that the back map falls on the unperturbed map when $p_n=p_0$, even though p has been changed during both the current and previous oscillations. In other words, the location of the chaotic attractor depends only on the current p_n and not on the previous value of p. In this case recursive proportional feedback reduces to the simple proportional feedback algorithm of Ref. 18:

$$\delta p_n=-\tilde{K}\delta x_n, \tag{9a}$$

$$\tilde{K}=-\frac{\mu}{\nu}. \tag{9b}$$

Thus the experimental procedure for finding μ, ν, and ω also provides a predictor for the likelihood that the simpler control algorithm is applicable and the recursive term in recursive proportional feedback is unnecessary.

Simple proportional feedback effectively controls chaos in many systems whose dynamics exhibit a 1D return map. For example, we can use simple proportional feedback to stabilize chaotic oscillations that are solutions of the Lorenz equations.[28] See the Appendix for more details. However, simple proportional feedback cannot control chaotic dynamics in some systems even though the dynamics are highly dissipative (that is, reducible to a 1D mapping). In particular, using simple proportional feedback as a control strategy with $\tilde{K}$ set according to Eq. (9b), we failed to control chaotic oscillations in the KSS circuit for the parameters of our experiment. As Fig. 4 clearly shows, the back map does not coincide with the unperturbed map for the KSS circuit, which explains why simple proportional feedback with $\tilde{K}=-\mu/\nu$ is not likely to achieve control for this system. If we follow the more general formulation of Ref. 3, we can show that the speed with which a system with simple proportional feedback and $\tilde{K}$ specified by Eq. (9b) approaches control increases as $|\omega\tilde{K}|\to 0$. We can also show that simple proportional feedback with $\tilde{K}=-\mu/\nu$ must fail for $|\omega\tilde{K}|\geqslant 1$.

IV. RECURSIVE PROPORTIONAL FEEDBACK APPLIED TO A SIMPLE ELECTRONIC OSCILLATOR

To apply the recursive proportional feedback algorithm to the KSS circuit, we must acquire the output voltage x and supply the perturbed control voltage p after each oscillation. To do so, we can choose from a wide variety of programable data acquisition systems. For our experiment, we created programs in LabVIEW[29] to control a National Instruments data acquisition board that interfaced with the circuit. We acquired data at 50 Hz, a frequency that is sufficiently high to resolve the approximately 1 Hz signal and low enough to allow sufficient time between data points to implement the recursive proportional feedback algorithm. The precision of the measured signal was 0.3 mV. After each data point, the program determined whether a local maximum of x had been acquired. A local maximum is identified when the previous

Table I. Calculated values of the quantities used to implement the recursive proportional feedback algorithm for the KSS circuit from experimental measurements of the output voltage x.

x_F	1.777±0.007 V
x_F^u	1.833±0.010 V
x_F^b	1.810±0.008 V
μ	−1.604±0.010
ν	2.92±0.64
ω	1.72±0.55
K	0.87±0.34
R	−0.93±0.57

voltage value is larger than both its previous and the current value. This simple test never returned false peaks because the noise in the circuit was sufficiently small. When control was turned on, the program used the recursive proportional feedback algorithm, Eq. (6), to calculate the voltage perturbation δp and update the value of $p=p_0+\delta p$ that was input to the circuit via the digital-to-analog output of the board. Because the perturbations must be small enough so that the linear approximation Eq. (4) is valid, the perturbations were set to zero if $|\delta p_n|>\epsilon$. For our experiment, $p_0=1.0000$ V and $\epsilon=0.05$ V. The precision of the input voltage p was 0.3 mV, which is an order of magnitude smaller than values of the perturbations δp. From the experimentally generated return maps shown in Fig. 4, we calculated the values of quantities needed for the recursive proportional feedback algorithm, which are shown in Table I. The uncertainties in these quantities are propagated from the uncertainties in least squares fits to the return maps.

The effect of the recursive proportional feedback algorithm on the signal is dramatically evident in Fig. 5, which shows the oscillating output voltage $x(t)$ versus time. Perturbations to the control parameter p began slightly before $t=20$ s. Before control is turned on, the oscillations vary aperiodically with a wide range in amplitude. After control is turned on, the voltage oscillates periodically with nearly constant amplitude. Figure 6 shows a sequence of the maxima x_n of the output voltage for an experimental run in which control was turned on and then turned off. Before control, the values of the maxima vary widely with a range of about 0 to 2.6 V. After control is turned on at $n=140$, the maxima

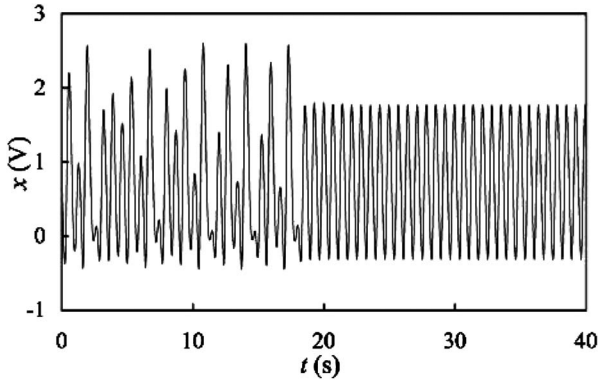

Fig. 5. Oscillating output voltage $x(t)$ of the circuit versus time. Control was turned on slightly before 20 s. For visualization purposes, the data was sampled at 1 kHz.

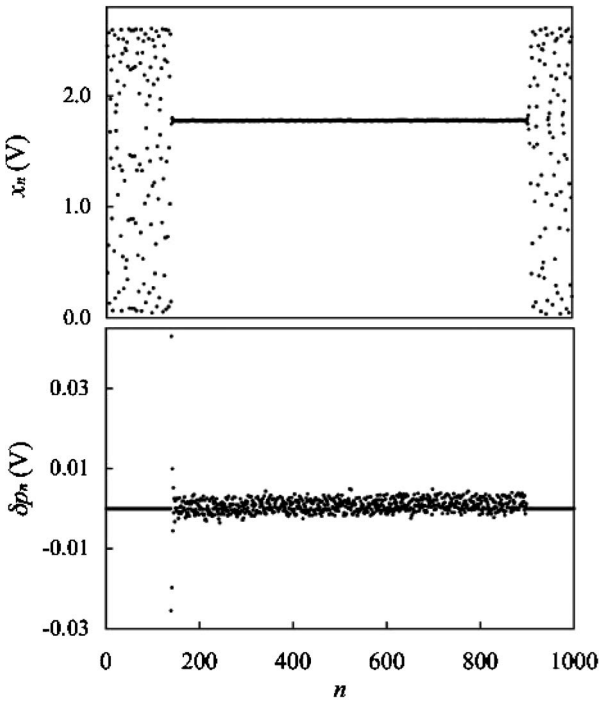

Fig. 6. A sequence of oscillation maxima x_n for an experimental run for which control was turned on at $n=140$ and turned off at $n=900$. The corresponding sequence of control perturbations δp_n is also shown.

have a nearly constant value very close to the target fixed point. The average of the actual maxima is $\bar{x}_n=1.778$ V, which is within the uncertainty of $x_F=1.777\pm0.007$ V. The standard deviation in the measured values of the maxima during control equals 0.002 V and is only 0.25% of the standard deviation of the maxima without control. When control is turned off at $n=900$, the maxima again vary widely. Figure 6 also shows the values of perturbations δp applied to the control parameter. Control was achieved immediately after the perturbations were generated and was lost once the perturbations were stopped. Control is achieved with remarkably small perturbations. The average absolute value of δp is only 1.4 mV, which means that the input current to the circuit during control is only increased or decreased on average by 0.14% of the input current with no control.

V. CONCLUSIONS

We have derived the recursive proportional feedback algorithm and shown that it can be used to control chaotic oscillations in the Kiers, Schmidt, and Sprott electronic circuit. Control is achieved with small perturbations and the mean oscillation maximum during control is well within the uncertainty of the target fixed point. The values of the coefficients used in the recursive proportional feedback algorithm were calculated from experimentally measured values of the output voltage of the circuit during precontrol measurements. Recursive proportional feedback is suitable for highly dissipative systems, of which the KSS circuit is an example. Simple proportional feedback is also suitable for some highly dissipative systems, but cannot be used for the KSS circuit because the movement of the system's chaotic attractor through phase space depends on both the current and previous perturbations.

ACKNOWLEDGMENTS

This material is based upon work supported by the National Science Foundation under Grant Nos. 0241814 and 0241890 and by an award from Research Corporation.

APPENDIX: SUGGESTIONS FOR FURTHER STUDY

Problem 1. Write a program to control the logistic map using simple proportional feedback, Eq. (9). The logistic map is defined as

$$x_{n+1} = f(x_n,p) = px_n(1 - x_n). \tag{A1}$$

This map behaves chaotically for $3.57 < p \leqslant 4$, except for small windows of periodicity. Choose a value such as $p_0 = 3.9$ for the unperturbed value of the system parameter. The fixed point x_F and derivatives μ and ν in Eq. (9) can be determined analytically without recourse to numerical data (see Ref. 5 for details on the derivation of simple proportional feedback for the logistic map). Iterate the logistic map a few hundred times without control to insure steady state chaotic behavior and then turn on control by updating $p = p_0 + \delta p$ after each iteration. Investigate what happens when the control is turned off.

Problem 2. Write a program to control the Lorenz oscillator using recursive proportional feedback, Eq. (6). The equations for the Lorenz oscillator are given by[28]

$$\dot{x} = \sigma(y - x), \tag{A2a}$$

$$\dot{y} = rx - y - xz, \tag{A2b}$$

$$\dot{z} = xy - bz, \tag{A2c}$$

where σ, r, and $b > 0$ are system parameters. The dynamical variables x, y, and z behave chaotically for wide ranges of these parameters. Use r as the perturbation parameter to implement chaos control and choose $\sigma = 10$, $r_0 = 28$, and $b = \frac{8}{3}$. Numerically solve Eq. (A2) and treat the numerical solution for the dynamical variable z as experimental data. Find the sequence of maximum values of z. Follow the procedure in Sec. III for constructing unperturbed, up, and back return maps from this sequence and use these maps to find the fixed point z_F and derivatives μ, ν, and ω that determine K and R. If $\omega \approx 0$, try neglecting the recursive term in Eq. (6) and controlling the Lorenz oscillator using simple proportional feedback, Eq. (9).

Problem 3. Construct a chaotic oscillator using a nonlinear subcircuit $D(x)$ other than the one used in the KSS circuit. See Ref. 23 for several options for $D(x)$. For example, build a circuit with $D(x) = |x|$. Explore the chaotic dynamics of this circuit and compare the experimental output to numerical solutions of Eq. (2). Try to control chaos in this circuit using recursive proportional feedback.

Problem 4. Follow the control theory formulation of Ref. 3 and show that the linearized evolution of a highly dissipative system, subject to a 1D return map, may be expressed by the matrix equation:

$$\begin{pmatrix} x_{n+1} - x_F \\ p_n \end{pmatrix} = \begin{pmatrix} \mu + \nu K & \omega + \nu R \\ K & R \end{pmatrix} \begin{pmatrix} x_n - x_F \\ p_{n-1} \end{pmatrix}. \tag{A3}$$

Derive the recursive proportional feedback expressions for K and R, Eq. (5), by requiring both of the eigenvalues of the transformation matrix to be zero. For the values of μ, ν, and ω used in this paper, find the range of values of K and R that will achieve control (that is, those for which the eigenvalues of the transformation matrix have absolute values less than 1).

[a]Electronic address: wienerr@pacificu.edu

[1] S. H. Strogatz, *Nonlinear Dynamics and Chaos: With Applications to Physics, Biology, Chemistry, and Engineering* (Perseus Books, Cambridge, MA, 1994).
[2] E. Ott, C. Grebogi, and J. A. Yorke, "Controlling chaos," Phys. Rev. Lett. **64**(11), 1196–1199 (1990).
[3] F. J. Romeiras, C. Grebogi, E. Ott, and W. P. Dayawansa, "Controlling chaotic dynamical systems," Physica D **58**, 165–192 (1992).
[4] K. Ogata, *Modern Control Engineering* (Prentice Hall, Upper Saddle River, NJ, 1997), 3rd ed.
[5] D. J. Gauthier, "Resource letter: CC-1: Controlling chaos," Am. J. Phys. **71**, 750–759 (2003).
[6] W. L. Ditto, S. N. Rausseo, and M. L. Spano, "Experimental control of chaos," Phys. Rev. Lett. **65**, 3211–2314 (1990).
[7] J. Starrett and R. Tagg, "Control of a chaotic parametrically driven pendulum," Phys. Rev. Lett. **66**, 1974–1977 (1995).
[8] J. Singer, Y.-Z. Wang, and H. H. Bau, "Controlling a chaotic system," Phys. Rev. Lett. **66**, 1123–1125 (1991).
[9] E. R. Hunt, "Stabilizing high-period orbits in a chaotic system: The diode resonator," Phys. Rev. Lett. **67**, 1953–1955 (1991).
[10] R. Roy, T. Murphy, Jr., T. D. Majer, Z. Gills, and E. R. Hunt, "Dynamical control of a chaotic laser: Experimental stabilization of a globally coupled system," Phys. Rev. Lett. **68**, 1259–1260 (1992).
[11] P. Parmananda, P. Sherard, R. W. Rollins, and H. D. Dewald, "Control of chaos in an electrochemical cell," Phys. Rev. E **47**, R3003–R3006 (1993).
[12] P. Parmananda, R. W. Rollins, P. Sherard, and H. D. Dewald, "Recursive proportional-feedback and its use to control chaos in an electrochemical system," in *Proceedings of the 2nd Conference on Experimental Chaos*, edited by W. Ditto, L. Pecora, S. Vohra, M. Shlesinger, and M. Spano (World Scientific, River Ridge, NJ, 1995), pp. 304–316.
[13] A. Garfinkel, M. L. Spano, W. L. Ditto, and J. N. Weiss, "Controlling cardiac chaos," Science **257**, 1230–1235 (1992).
[14] R. J. Wiener, D. C. Dolby, G. C. Gibbs, B. Squires, T. Olsen, and A. M. Smiley, "Control of chaotic pattern dynamics in Taylor vortex flow," Phys. Rev. Lett. **83**, 2340–2343 (1999).
[15] P. Kolodner, G. Flätgen, and I. G. Kevrekidis, "Controlling dispersive chaos in binary-fluid convection," Phys. Rev. Lett. **83**, 730–733 (1999).
[16] G. L. Baker, "Control of the chaotic driven pendulum," Am. J. Phys. **63**, 832–838 (1995).
[17] U. Dressler and G. Nitsche, "Controlling chaos using time delay coordinates," Phys. Rev. Lett. **68**, 1–4 (1992).
[18] B. Peng, V. Petrov, and K. Showalter, "Controlling chemical chaos," J. Phys. Chem. **95**, 4957–4959 (1991).
[19] R. W. Rollins, P. Parmananda, and P. Sherard, "Controlling chaos in highly dissipative systems: A simple recursive algorithm," Phys. Rev. E **47**, R780–R783 (1993).
[20] C. Flynn and N. Wilson, "A simple method for controlling chaos," Am. J. Phys. **66**, 730–735 (1998).
[21] Ned J. Corron, Shawn D. Pethel, and Buckley A. Hopper, "A simple electronic system for demonstrating chaos control," Am. J. Phys. **72**, 272–276 (2004).
[22] K. Kiers, D. Schmidt, and J. C. Sprott, "Precision measurements in a simple electronic circuit," Am. J. Phys. **72**, 503–509 (2004).
[23] J. C. Sprott, "Simple chaotic systems and circuits," Am. J. Phys. **68**, 758–763 (2000).
[24] J.-C. Roux, R. H. Simoyi, and H. L. Swinney, "Observation of a strange attractor," Physica D **8**, 257–266 (1983).
[25] R. W. Rollins and E. R. Hunt, "Exactly solvable model of a physical system exhibiting universal chaotic behavior," Phys. Rev. Lett. **49**, 1295–1298 (1982).
[26] An interesting feature of the return map for the KSS circuit is that the thin 1D curve bends back near itself, creating closely separated lower and upper branches (see Fig. 9 in Ref. 22), which are not resolved by the scale used in Fig. 3. Thus there are two intersections of the map and the $x_{n+1} = x_n$ line, which means there are two unstable period-one fixed points. We used recursive proportional feedback to stabilize the lower-branch fixed

point. We were not able to gain control for the upper-branch fixed point, which suggests that it is not a saddle point. See Ref. 1 for details on classifying fixed points and Ref. 16 for a discussion of why a saddle point is needed for proportional feedback control.

[27] If the sequence is generated with the odd values of x corresponding to $p=p_0$ and the even values corresponding to $p=p_0+\Delta p$, then the up map consists of x_2 plotted against x_1, x_4 plotted against x_3, and so on; the back map consists of x_3 plotted against x_2, x_5 plotted against x_4, and so on.

[28] E. N. Lorenz, "Deterministic nonperiodic flow," J. Atmos. Sci. **20**, 130–141 (1963).

[29] A concise, user-friendly text on LabVIEW and computer-based data acquisition is by John Essick, *Advanced LabVIEW Labs* (Prentice Hall, Upper Saddle River, NJ, 1999). It culminates with a chapter on developing a temperature control system that uses a proportional feedback algorithm that is appropriate for linear systems.

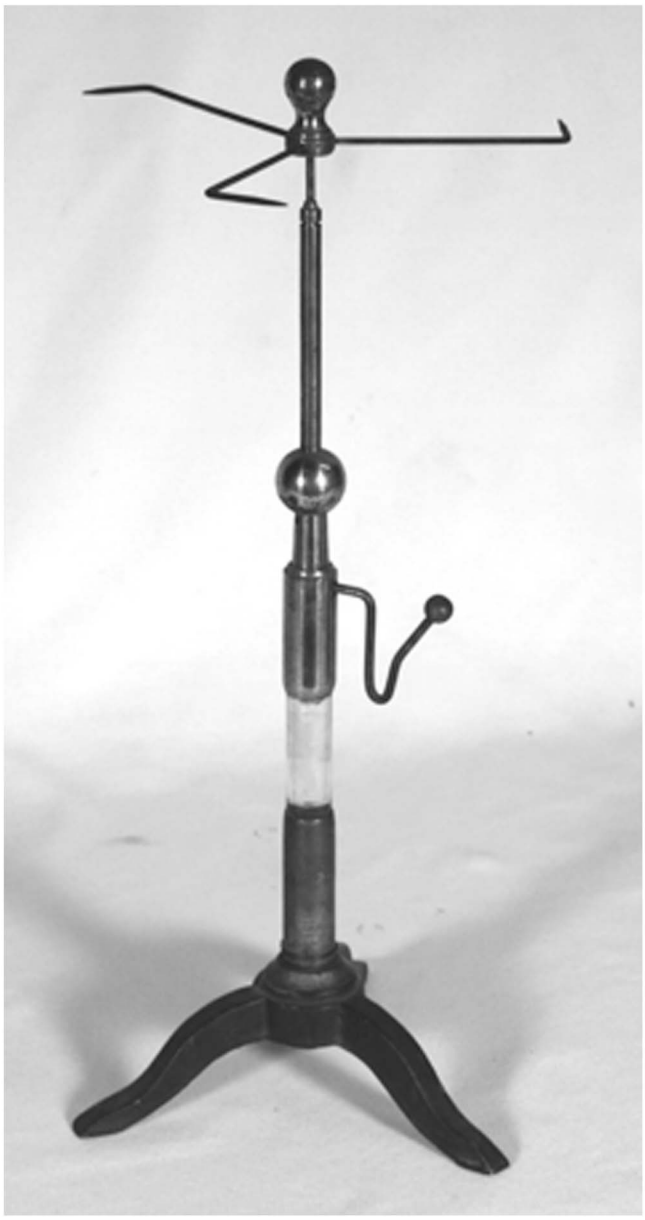

Electric Fly. The Electric Fly is made of a number of brass wires, with rearward-facing sharp points, joined at a hub. This is pivoted atop an insulated shaft. One terminal of an electrostatic machine is connected to the whirl and the other is grounded. As the charge builds up on the metallic parts of the whirl, the equipotential lines are bunched together at the sharp points, creating a large electric field there. Eventually the field becomes large enough to ionize the air molecules and create a space charge that is of the same sign as the point. The mutual repulsion between the space charge and the point causes the wheel to spin. This example, in the Greenslade Collection, runs well with either a Wimshurst machine or a Van de Graaff generator. (Photograph and Notes by Thomas B. Greenslade, Jr., Kenyon College)